Journal of Membrane Science 640 (2021) 119844

Contents lists available at ScienceDirect

Journal of Membrane Science

journal homepage: www.elsevier.com/locate/memsci

Electrochemical manufacture of graphene oxide/polyaniline conductive membrane for antibacterial application and electrically enhanced water permeability

Bojun Li [a,b,1], Wenjing Tang [a,c,1], De Sun [a,*], Bingbing Li [a,**], Yanxia Ge [a,***], Xin Ye [d], Wei Fang [d]

[a] Department of Chemical Engineering, Changchun University of Technology, 2055 Yanan Street, Changchun, 130012, PR China
[b] State Key Laboratory of Water Environment Simulation, School of Environment, Beijing Normal University, Beijing, 100875, PR China
[c] Beijing Key Laboratory of Farmland Soil Pollution Prevention and Remediation, College of Resources and Environmental Sciences, China Agricultural University, Beijing, 100193, PR China
[d] Changchun Institute of Optics, Fine Mechanics and Physics, Chinese Academy of Sciences, Changchun, 130012, PR China

ARTICLE INFO

Keywords:
Graphene oxide
Polyaniline membrane
Electrochemical preparation
Water permeability
Antibacterial

ABSTRACT

Electrofiltration, an effective approach for membrane fouling mitigation, is significantly limited by membrane properties. A facile electrochemical method was proposed to fabricate the graphene oxide/sulfuric acid-doped polyaniline (GO/S-PANI) membrane. For which, charging the graphite in H_2SO_4 (98 wt%) to obtain graphite intercalation compound (GIC), then in a mixed electrolyte (H_2SO_4, $CuSO_4$, $(NH_4)_2SO_4$), GO was exfoliated and assembled concurrently on the PANI membrane, which was doped by H_2SO_4 simultaneously. The introduction of Cu^{2+} made the GO layers on the membrane stable. Also, the GO/S-PANI membrane showed higher conductivity (55.6 S m^{-1}) than the PANI membrane (0.019 S m^{-1}). Moreover, GO/S-PANI membrane possessed a more applicable pore structure and improved hydrophilicity. As a result, membrane rejection increased, and the resistance to the negatively charged pollutants was enhanced. For 1 V electrofiltration of yeast suspension, water permeation was sustainably raised by using GO/S-PANI membrane than PANI membrane. The GO/S-PANI membrane was more stable with 1 V than without electric fields. The antibacterial rate can reach 92.1% for the GO/S-PANI membrane against Escherichia coli. Overall, our strategy provides a facile preparation method for the GO/S-PANI conductive membrane with application potential in electrofiltration and antibacterial fields.

1. Introduction

Membrane fouling is a primary problem that limits the wide use of membrane separation technology [1]. Typical pollutants in water, such as microbes, can deposit on and adhere to the membrane surface and then grow to form communities known as biofilms, allowing various bacteria to inhabit [2]. As microorganisms with inherent electronegativity can be affected by electrostatic force, recently, inhibiting microbial contamination of membranes through electrofiltration has become a research hotspot [3–6]. The research on electrofiltration proves that applying conductive membranes as the electrode with low-intensity electric fields can markedly enhance water permeation and decrease energy demand. Electrostatic force can be generated between membrane surface and the negatively charged microorganisms when electric fields are used. Thus, membrane fouling can be mitigated by reducing the adsorption potential of microorganisms [5,7–9].

Commonly, conductive membranes are fabricated by conductive materials such as carbons (e.g., graphene and carbon nanotube), metals (e.g., Au, Ag, and stainless steel), and conductive polymers (e.g., Polyaniline and Polypyrrole) [7,10–15]. However, since carbon membranes or metal membranes are high in cost and complex in preparation, carbon/conductive polymer composites are considered emerging materials for preparing conductive membranes. The membranes can combine the advantages of carbon and polymer materials and can be well utilized in electrofiltration processes [5,8,16]. It should be noted that, for the water treatment coupled with electric field, conductive membranes must have

* Corresponding author.
** Corresponding author.
*** Corresponding author.
E-mail addresses: sunde@ccut.edu.cn (D. Sun), lbingbing2002@163.com (B. Li), 79533880@qq.com (Y. Ge).
[1] Co-first authors: Bojun Li; Wenjing Tang.

https://doi.org/10.1016/j.memsci.2021.119844
Received 17 June 2021; Received in revised form 13 August 2021; Accepted 5 September 2021
Available online 9 September 2021

good stability under aqueous and harsh conditions (e.g., high pressure). Thus, only a limited number of conducting polymers (e.g., Polypyrrole, Polythiophene, and Polyaniline) can be used to fabricate conductive membranes [17]. The cost of pyrrole monomer is high, and the commercially available polythiophenes are few, so their extensive application in conductive polymer membranes was limited [16]. Polyaniline (PANI), a conductive polymer, has many advantages: relatively low cost, product marketization, controllable conductivity, and excellent environmental stability. It has been extensively studied and fabricated into conductive membranes by the nonsolvent induced phase separation (NIPS) method [12,17–19]. For the preparation of PANI membranes, sulfur-containing acids can be introduced as acid dopant to enhance membrane conductivity [5]. In terms of this, using poly (2-acrylamido-2-methyl-1-propanesulfonic acid) as a dopant, Xu et al. [20] have fabricated PANI conductive membranes revealing a conductivity of 0.1 S m^{-1} for the cross-flow filtration. Dodecylbenzene sulfonic acid was utilized by Wang et al. [12] to manufacture the PANI conductive membrane with a conductivity of 2.2 × 10^{-2} S m^{-1} for electrofiltration. Apart from these, the sulfur-containing acids can also improve the antifouling behavior and the chlorine resistance of the PANI membranes and increase membrane hydrophilicity [21,22]. The PANI membranes, doped by sulfur-containing acids, can also present tunable transport properties for water and solute when additionally doped by HCl [22].

Graphene-based materials are among the most widely used carbon materials to manufacture separation membranes [14,23–26]. Although pristine graphene typically possesses better conductivity than graphene oxide (GO), due to the existence of functional hydrophilic groups and the physical piercing of edges, GO has exhibited excellent performance for membrane fouling mitigation [7,23]. In antibacterial field, GO also revealed a better effect than pristine graphene [24]. Additionally, only limited interaction force (e.g., π-π interaction) can be generated when the pristine graphene was combined with PANI membrane, leading to the restricted stability of graphene on the membrane [27]. In contrast, GO and PANI can be combined tightly through electrostatic interactions, hydrogen bonding, and π-π stacking, providing a good foundation for preparing composites [28,29]. By way of example, firstly through the Hummers' method to obtain GO, then the GO/PANI reinforced hollow fiber membranes were prepared for the preconcentration of the Ivermectin [30]. Employing a modified Hummers' method to synthesize initial GO, then a GO/PANI nanocomposite membrane was developed for CO_2/N_2 separation [31]. Through the Hummers' method combined with an in-situ polymerization, a PANI/GO nanocomposite was designed for room-temperature thermoelectric enhancement [32]. Although GO/PANI composites have been extensively prepared, currently GO is mostly prepared through chemical oxidation, such as the Hummers' method [33] and the modified Hummers methods [34], which may bring safety risks and cause environmental issues [35]. Most recently, through the technique of electrochemical oxidation and exfoliation, GO production becomes safe in operation and simple in the process [36–38]. For instance, after graphite intercalation compounds (GICs) were obtained by charging the commercial graphite foil in the concentrated H_2SO_4, Cao et al. [36] produced GO through a short time electrochemical oxidation and exfoliation of GICs in 0.1 M $(NH_4)_2SO_4$ solution. As an alternative approach, using a similar step to prepare GICs, Pei et al. selected the diluted H_2SO_4 (50 wt%) as the electrolyte to oxidize and exfoliate GICs into GO [37]. Nevertheless, very few studies focus on the fabrication of GO composite membranes directly using graphite/intercalated graphite as the precursor. In the fields of electrofiltration and antibacterial, it is critical to develop a facile electrochemical method to produce the conductive GO/PANI membranes with high performance.

In this study, GO/sulfuric acid-doped PANI (GO/S-PANI) membranes were developed by a modified electrochemical method. The graphite foil was electrochemically intercalated to prepare GICs, then, GO was produced and assembled on the PANI membrane, which was doped by sulfuric acid simultaneously. Membrane properties were analyzed, and membrane fouling mitigation's impact on water permeability for the electrofiltration processes was studied. The facile electrochemical preparation method of the GO/S-PANI membrane has shown multiple advantages: (1) In contrast to the GO prepared by the Hummers/modified Hummers' method, there are no explosive reactions, and the production of GO is high [36,37]. (2) In the electrochemical intercalation step, the sulfuric acid electrolyte can be reused until fully consumed, as this step generates no contaminants [36]. (3) Contributing to the forming of the expanded spaces among layers and the large volume of the water channels, the GO layers assembled on the membrane will not be compacted as it happens during vacuum filtration [39,40]. (4) For GO composite membranes, the fabrication method often requires two steps (the preparation of GO and then the combination of GO with membranes); for the PANI membranes prepared by the NIPS method, an extra step of acid immersion was needed to increase membrane conductivity [12,31]. By this electrochemical approach, the three processes, including the preparation of GO, the assembly of GO on the PANI membrane, and the acid doping of the PANI membrane can be proceeded concurrently. This study provides an innovative strategy for preparing acid-doped GO/PANI membrane, promisingly used in electrofiltration and antibacterial fields.

2. Experimental methods

2.1. Materials

Commercial PANI polymer (Emeraldine base, Molecular weight: 10,000–100000, Purity: ≥ 99.0 wt%, Particle size: less than 30 μm by laser particle analyzer; 100 nm by TEM) was purchased from Cool Chemical Technology (Beijing) Co., Ltd. (China). Ammonium Sulfate, Sulfuric acid, N-methyl-2-pyrrolidone (NMP), 4-methyl piperidine (4-MP), and Copper (II) sulfate pentahydrate ($CuSO_4{\cdot}5H_2O$) were provided by Sigma-Aldrich (UK). Graphite foil was acquired from Qingdao Herita Graphite Products Co., Ltd. (China). PET non-woven fabric was supplied by Haoxin Insulation Materials Co., Ltd. (China). Dry yeast was obtained from Angel Yeast Co., Ltd. (China). Deionized (DI) water was prepared from the laboratory-made. All chemical reagents were used as received without any purification.

2.2. PANI membrane fabrication

PANI membrane was prepared via the NIPS method (Fig. 1a) at room temperature [41]. In a nutshell, 2.64 g 4-MP and 15.4 g NMP were mixed, then 3.96 g PANI powder was slowly introduced into the mixture. The mixture was continuously stirred at a high speed of 300 rpm for 4 h to produce the homogeneous PANI solution. Next, cast the mixed solution on the non-woven fabric, tiled on a smooth glass plate. The casting thickness was 420 μm that the large thickness brought good mechanical properties. After being exposed to the atmosphere for 30 s, the membrane was immersed in the coagulation bath, which used DI water as the nonsolvent and stayed there for at least 24 h. At last, the generated membrane was rinsed with fresh water and stored in DI water for later use.

2.3. Electrochemical preparation of GO/S-PANI membrane

The electrochemical process for preparing graphite intercalation compound (GIC) was shown in Fig. 1b. GIC was synthesized by charging a strip of graphite foil (Fig. 1c, 4 × 5 cm^2) under 2 V for 15 min. In this process, the graphite foil and platinum sheet were used as the anode and the cathode, respectively; concentrated sulfuric acid (98 wt%, 200 ml) was selected as the electrolyte (Fig. 1d). The intercalation of sulfuric acid made graphite foil expanded and turned into a blue color which indicated the formation of GIC (Fig. 1e) [36]. The GIC was still robust mechanically allowing it move from one electrode device to another for

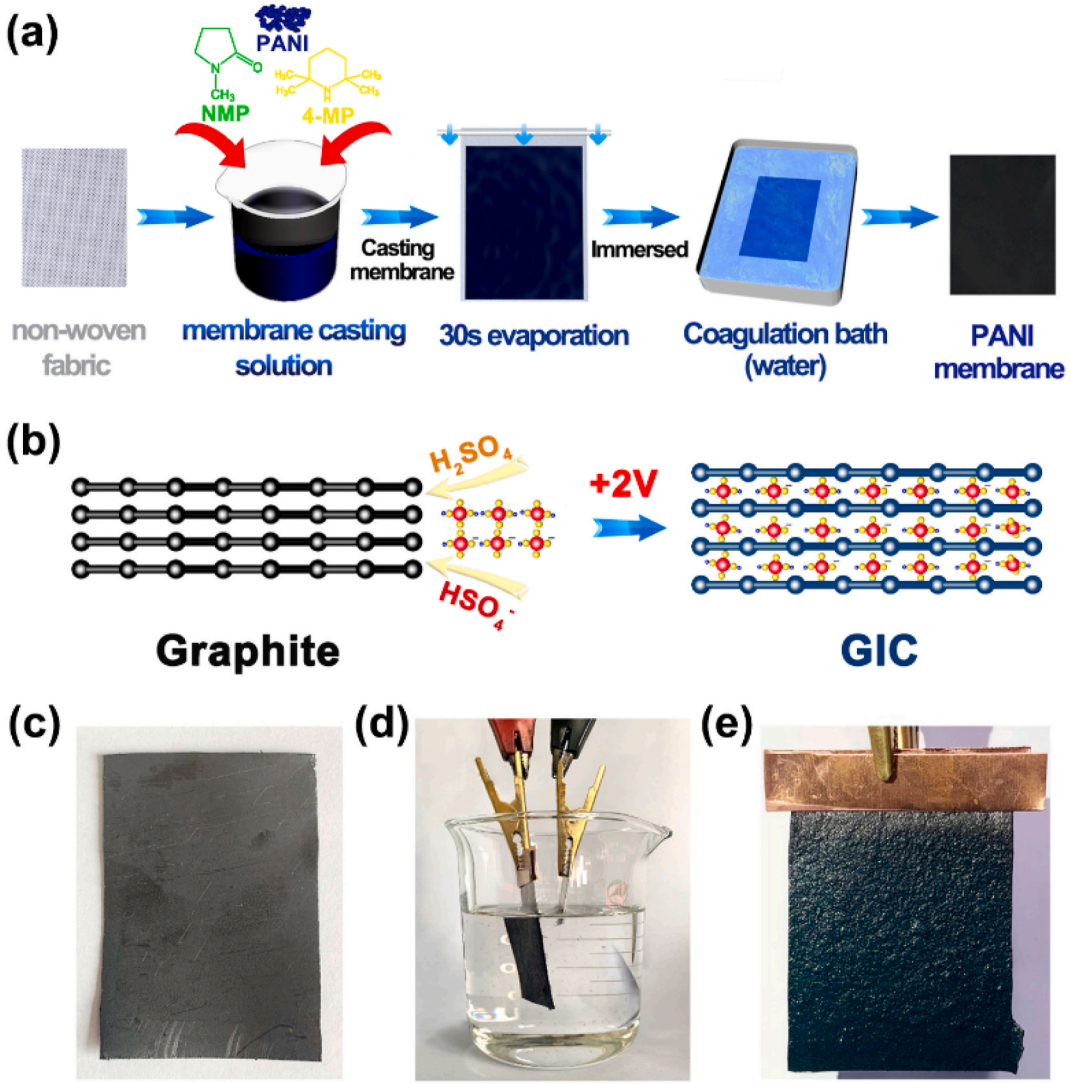

Fig. 1. (a) Schematics of the preparation procedure for PANI membrane. (b) Schematic illustration of the electrochemical intercalation for the production of GIC. (c) Photographs of graphite (4 × 5 cm^2 in the area). (d) Electrode setup for oxidation of GIC. (e) Photographs of graphite foil (4 × 5 cm^2 in area and 0.3 mm in thickness) being charged to 2 V, forming a blue in color GIC. (For interpretation of the references to color in this figure legend, the reader is referred to the Web version of this article.)

further treatment.

Fig. 2a illustrated the electrochemical process for the fabrication of the GO/S-PANI membrane. The details are as follows: the newly prepared GIC and the PANI membrane (Fig. 2b left, 4 × 5 cm^2) were utilized as the anode and the cathode, respectively. They were placed vertically in 0.1 M $(NH_4)_2SO_4$ electrolyte with a distance of 1 cm. After that, set the power supply to 5 V and stabilized it for 120 min. The 0.001 M $CuSO_4$ solution was added to the electrolyte every 10 min (Fig. 2d), then the GO/S-PANI membrane (Fig. 2b right) was successfully obtained.

2.4. Mechanism of the electrochemical process for GO/S-PANI membrane preparation

When the voltage is applied in the above electrochemical process, the nucleophilic water molecules could immediately embed into GIC. The graphene layers within GIC then react with the nucleophilic water molecules and form –OH, C–O-, and C═O groups. The gaseous oxygen was produced by the oxidation of the intercalated water, leading to the volume expansion of GIC and then the dissociation/exfoliation of GO from GIC [36,37]. Additionally, the concentrated sulfuric acid intercalated in the GIC can penetrate into the electrolyte. Thereupon, the PANI membrane can also be doped by sulfuric acid [42]. By weighing the mass of the original graphite foil and GIC, the calculated sulfuric acid content in the electrolyte was 1.1 mol/L. During the electrochemical process, the positively charged Cu^{2+} ions in the electrolyte automatically adsorbed the negatively charged GO (GO/Cu^{2+}), which made the GO/Cu^{2+} positively charged (Fig. 3a) [43,44]. Under the action of electric fields, the formed GO/Cu^{2+} moved onto the cathode and assembled on the PANI membrane to form the GO/S-PANI membrane. Through electrostatic interactions, hydrogen bonding, and π-π stacking, the GO layer was tightly combined with the PANI membrane (Figs. 2c and 3b) [28,29]. By this electrochemical strategy, the three processes, including the preparation of GO, the assembly of GO on the PANI membrane, and the acid doping of the PANI membrane can be proceeded concurrently, improving the experiment safety and simplifying membrane fabrication steps. The copper ions, confirmed as an excellent cross-linking agent for GO [45], could maintain mechanical stability and enhance water permeability of the GO layer. Meanwhile, the formed GO/Cu^{2+} on the GO/S-PANI membrane could increase antibacterial activity [46], which made contributions to the promotion of membrane mechanical stability and antibacterial ability.

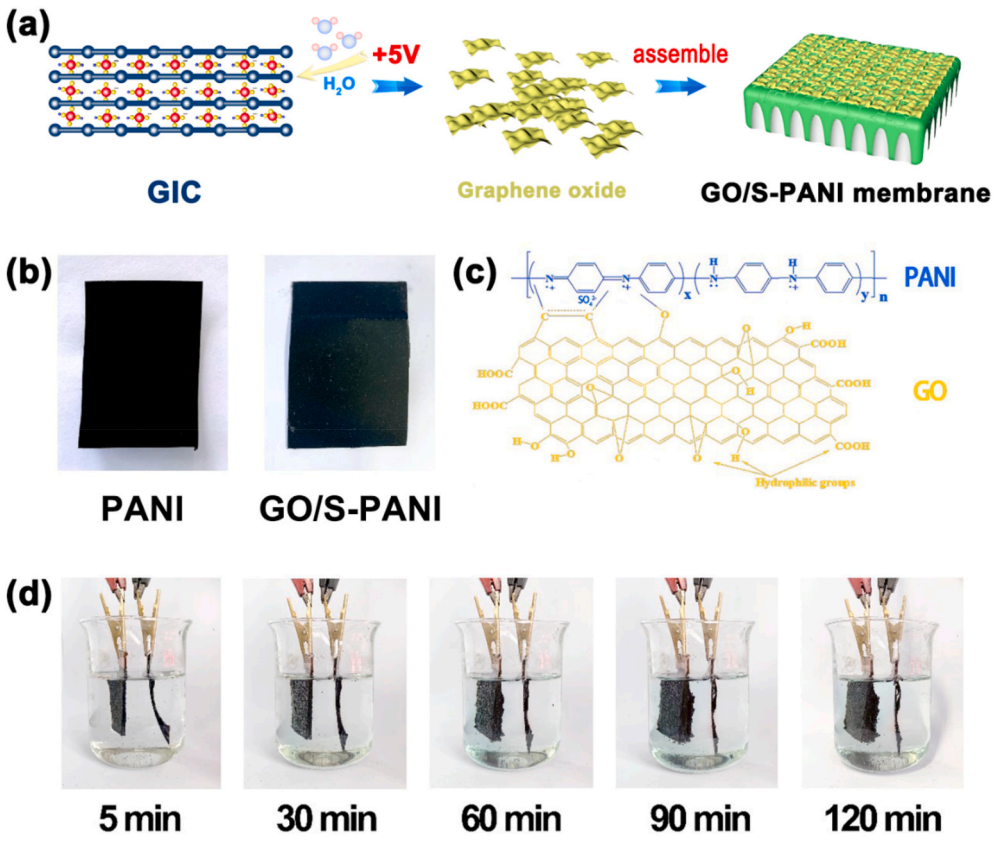

Fig. 2. (a) Schematic illustration of the electrochemical oxidation for GO production; assembly process of GO/S-PANI membrane. (b) Photographs of PANI membrane (4×5 cm^2 in the area) and GO/S-PANI membrane (4×5 cm^2 in the area). (c) Schematic illustration of the interaction between GO and PANI. (d) Photographs of the electrochemical preparation process for GO/S-PANI membrane.

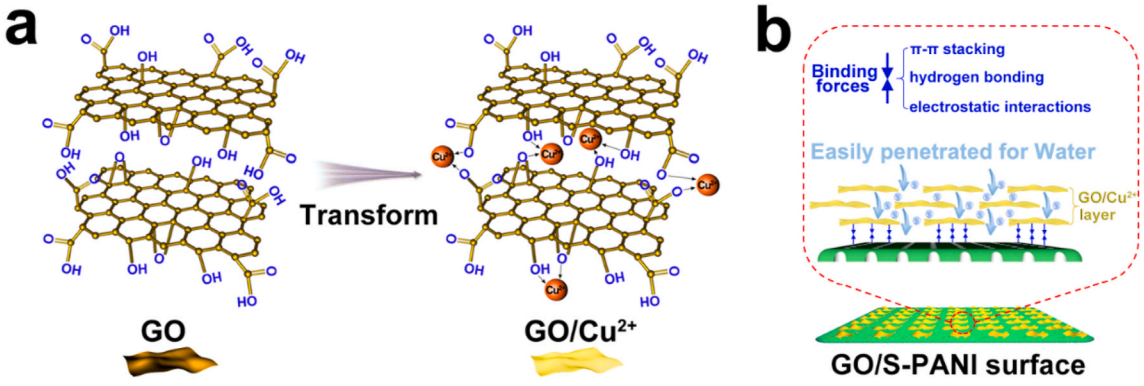

Fig. 3. (a) Schematic of GO formed into GO/Cu^{2+} (b) Binding forces between GO/S-PANI membrane and GO/Cu^{2+} layer.

2.5. Analytical method

Fourier transform infrared spectroscopy (FT-IR, Thermofisher Nicolet IS50FT-IR) was performed with the test wavelength 4000-525 cm^{-1}. Raman spectroscopy (Horiba Jobin Yvon LabRAM HR Evolution Raman spectrometer) was recorded from 200 to 4000 cm^{-1} using a 532 nm laser. X-ray Photoelectron Spectroscopy (XPS ESCALAD 250) was tested by Mg Kα X-ray source (1486 eV). The X-ray diffraction (XRD, Rigaku Smartlab X-ray Diffractometer) was investigated with the radiation of K beta filter method (45 kV, 200 mA) in a 2θ range of 5–70° with a step size of 0.01 and a sweep rate of 10° per minute. The membrane morphology and the distribution of the elements were recorded by SEM-EDX (JSM6510 JEOL). Membrane roughness was measured using the AFM (Agilent technologies AFM 5500) in tapping mode. The tensile test of membranes was carried out on a universal testing machine (YHS-229WG, Shanghai Yihuan Co, China). Pore size and pore size distribution (PSD) of the membranes were tested by the capillary flow porosimeter (POROLUX 500, Germany). Dynamic droplet contact angles were measured using a contact angle meter (HARKE-SPCA Beijing Hake Experimental Instrument Factory).

2.6. Evaluation of controlling water permeability by fouling mitigation

The change in permeation flux of the yeast suspension was an obvious indicator of evaluating the membrane fouling mitigation [8,47]. Fig. S1 showed the electrofiltration setup. The membrane module (Fig. S2) was made from non-conductive photosensitive resin materials with an effective permeation area of 3.24 cm^2. Fixing the membrane in

the membrane module (Fig. S3), titanium plate (3.5 × 3.5 cm^2) and conductive membrane were used as the anode and the cathode. A distance of 1 cm was placed for the two electrodes. A direct-current power supply was utilized to generate electric fields. Yeasts (Zeta potential: −12.9 mV, size: 2–5 μm, Fig. S4) were dissolved in tap water to prepare yeast suspension, and 2 L yeast suspension with a concentration of 2 g L^{-1} was used as the feed. With the application of electric fields, the permeation liquid was collected at 0.04 Mpa, 25 °C, and a feed flow rate of 1.6 L min^{-1}. Each set of tests was conducted in three cycles with each cycle continuing for 180 min. Each test was repeated three times to obtain the average value with errors as the final results. After each cycle of testing, using tap water to wash the membrane and the conductivity of the membranes was tested instantly.

The flux is calculated based on the following equation:

$$J = \frac{Q}{A\,\Delta t} \tag{1}$$

Where J is flux (L m^{-2} h^{-1}), Q is the volume of collected solution (L), A represents the effective membrane area (m^2), and Δt stands for the permeation time (h).

The enhanced rate of total permeation flux is calculated based on the following formula:

$$q = \frac{Q_2 - Q_1}{Q_1} \tag{2}$$

In the formula, q is the enhanced rate of total permeation flux (%), Q_1 is the total permeation flux of the GO/S-PANI membrane without electric fields (L), Q_2 stands for the total permeation flux of tested membranes under series of low-intensity electric fields (L).

Through UV–Vis spectrophotometer (Shanghai YOKE instrument), the yeast concentrations in the solutions are measured at a wavelength of 600 nm, the rejection rate (R) of yeast is calculated based on the following formula:

$$R(\%) = \left(\frac{C_f - C_p}{C_f}\right) \times 100\% \tag{3}$$

In the formula, R represents the rejection rate of membranes, C_p is the

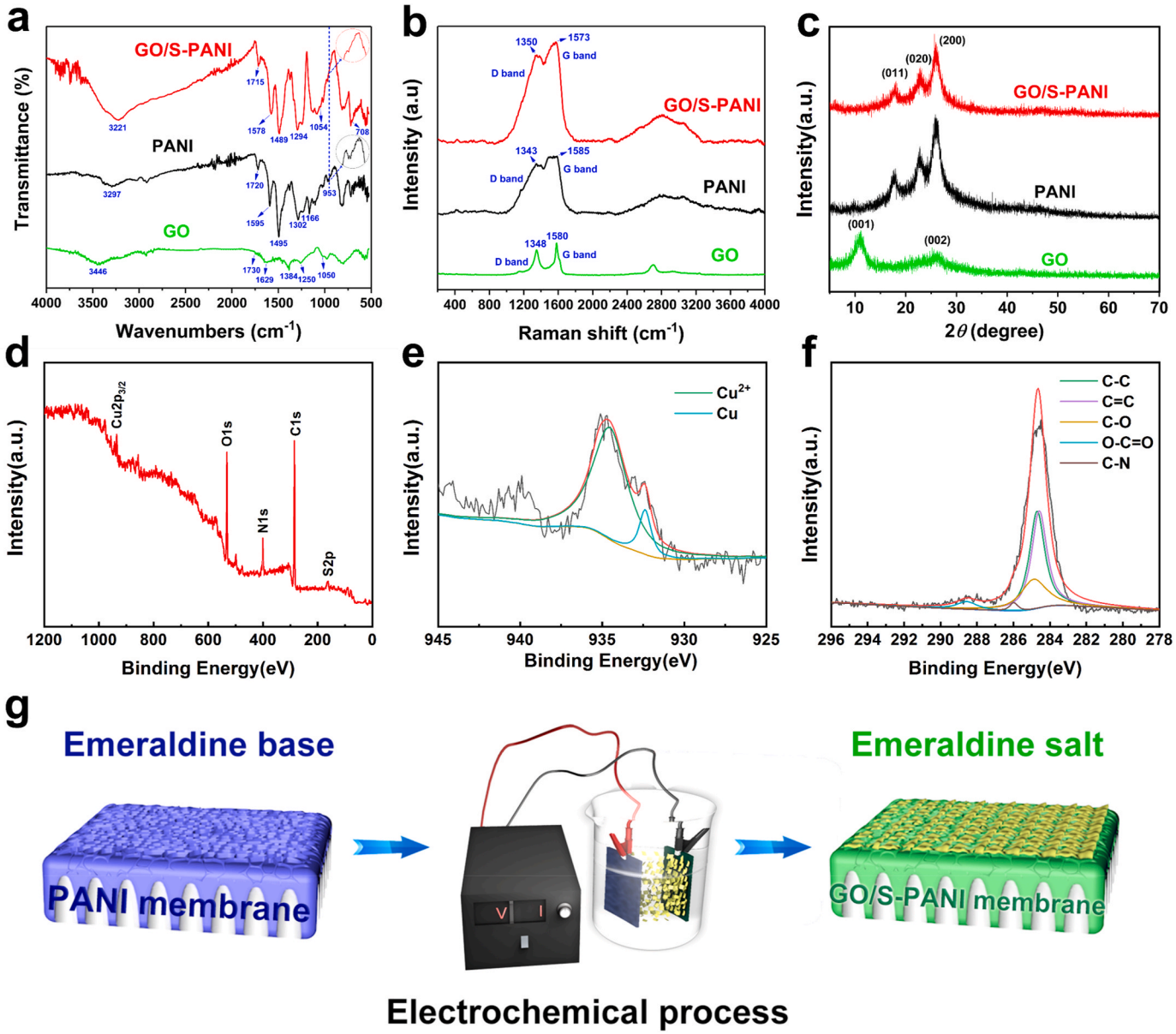

Fig. 4. Spectra of GO, PANI membrane, and GO/S-PANI membrane: (a) FTIR (b) Raman (c) XRD (d) XPS wide scan spectra (e) Cu 2p in XPS (f) C 1s in XPS (g) PANI converted from emeraldine base into emeraldine salt during the electrochemical process.

concentrations of the yeast in the permeation, and C_f is the concentrations of the yeast in the feed. As schemed in Fig. S5, the standard curve (a wavelength of 600 nm) was plotted for 2 g L^{-1} yeast suspension.

3. Results and discussion

3.1. Membrane characterization

3.1.1. Membrane chemical analysis

The FTIR spectra were represented in Fig. 4a. For GO samples, the absorption peak centered at 3446 cm^{-1} was attributed to the O–H stretching, and the other four peaks at 1629 cm^{-1}, 1384 cm^{-1}, 1250 cm^{-1}, and 1050 cm^{-1} belonged to the C═C, C–OH, C–O–C, and C–O stretching vibrations, respectively. Besides, the weak peak near 1730 cm^{-1} was related to the C═O in the carbonyl and carboxyl groups. The above peaks were consistent with the classic map, indicating the successful synthesis of GO [48,49]. According to PANI spectra, the peaks at 1595 cm^{-1} and 1495 cm^{-1} originated from the C═C and C═N stretching vibrations of the quinoid ring, respectively, revealing the PANI chains in emeraldine base form. The peak at 1302 cm^{-1} was related to the C–N stretching mode of the benzene unit, and 1166 cm^{-1} was attributed to the in-plane bending vibration of the benzene ring. In addition, the peak at 953 cm^{-1} was caused by the out-of-plane C–H deformation vibration of 1, 2, 4-disubstituted benzene [50,51]. By comparison, for the GO/S-PANI spectra, a broad peak was found at 3221 cm^{-1} attributing to the -NH^{2+} stretching, which demonstrated the protonation of PANI. The weak but identifiable peak at 1054 cm^{-1} represented the S═O stretching and the 708 cm^{-1} was related to the S–O stretching, confirming the existence of the sulfuric acid doping in the PANI of GO/S-PANI [52]. Meanwhile, the peaks at 1578, 1489, and 1294 cm^{-1} were redshifted by 17, 6, and 8 cm^{-1}, respectively, and the peak at 1166 cm^{-1} disappeared compared with PANI, further reflecting GO/S-PANI membrane was in the emeraldine salt form [53,54]. Additionally, the peak of the GO/S-PANI membrane at 953 cm^{-1} disappeared, implying a bonding interaction between the nitrogen atom of PANI and the C═O group on GO [55]. A redshift from 1720 cm^{-1} in PANI to 1715 cm^{-1} in GO/S-PANI also confirmed that the carboxyl group of GO was connected to the PANI through the nitrogen atom of the PANI main chain [56].

As illustrated in Fig. 4b, for Raman spectra, the centers of the two characteristic D and G bands associated with the defect density in GO and the sp^2 bonding carbon bonds of the graphite sheet were at 1348 and 1580 cm^{-1}, respectively. The I_D/I_G ratio of Raman spectra was widely used to evaluate the quality of carbon materials. The ratio of GO was 0.81, indicating the existence of a few defects in the GO [57]. It can be observed that the D band at 1343 cm^{-1} for the PANI spectra was moved to a higher wavenumber of 1350 cm^{-1} for the GO/S-PANI spectra. It resulted from the interaction between the cationic radical species (C–N+) of PANI and the anionic radical species (COO-) of GO [58]. Furthermore, compared with PANI, the G band of the GO/S-PANI was sharper and moved from 1585 cm^{-1} to 1573 cm^{-1} caused by the resonance of the paired electrons N atoms in PANI with the adjacent benzene structures in GO [59]. Based on the above discussions, it can be confirmed that GO was successfully fabricated and assembled on the PANI membrane tightly. Besides, PANI was also converted from a semiconductor (emeraldine base) into a conductor (emeraldine salt) during the electrochemical process (Fig. 4g).

Phase structures of GO, PANI, and GO/S-PANI were investigated by XRD, as shown in Fig. 4c. The sharp peak for GO at $2\theta = 11°$ corresponded to the GO (001) crystal plane, indicating the presence of GO [48]. Furthermore, the peak observed at $2\theta = 26.5°$ (002) suggested the unoxidized state of graphene [60]. The XRD structure of the PANI sample was similar to that prepared by Sanches et al. [61]. For GO/S-PANI, the diffraction peaks at $2\theta = 18.0°$, $2\theta = 22.8°$, and $2\theta = 25.8°$ were exhibited, corresponding to the (011), (020), and (200) crystal planes of the emeraldine salt form of PANI, confirming the perfect formation of the hybrid system [32]. The peak appeared at $2\theta = 25.2°$ in PANI was shifted to $2\theta = 25.8°$ in GO/S-PANI, corresponding to the π-π stacking of the benzene ring and GO [32,62].

To analyze the elemental composition of GO/S-PANI membrane and the combination state of carbon and copper, further XPS spectra (Fig. 4d) were tested. Obvious peaks representing the elements C, O, N, S, and Cu were shown in GO/S-PANI, in which the existed S (168.0 eV) reflected the acid doping of PANI in GO/S-PANI. Besides, the XPS of C 1s (284.6 eV), N 1s (399.9 eV), and O 1s (531.8 eV) has appeared in GO/S-PANI. As shown in Fig. 4e, two signal peaks of Cu (933.1) and Cu^{2+} (935.1) were observed, reflecting the combination of Cu^{2+} and GO [63]. Meanwhile, the C 1s contained five signal peaks in Fig. 4f: C═C (284.2), C–C (284.6), C–O (284.9), C–N (286.2eV), and O–C═O (288.5) [64], demonstrating the existence of the abundant oxygen-containing functional groups on GO. To avoid the agglomeration caused by the coordination between the COO^- group on GO sheets and the positively charged Cu^{2+}, the added amount of copper ions must be sufficiently low. The Cu:C ratio was 0.072. The C:O ratio of the XPS has been widely used to evaluate the oxidation degree of GO, and the obtained ratio was 3:1, which confirmed that the GO with a small size and high oxidation degree was successfully prepared [65].

3.1.2. Membrane morphology and elemental analysis

The SEM images in Fig. 5 presented the surface morphology and the cross-section of the PANI and GO/S-PANI membranes. Both membranes shared similar cross-section structures, containing a dense surface layer and a sublayer with finger-like pores. The top surface morphology of the PANI membrane (PANI-a) revealed big crack-like pores (red circles) on the membrane surface. It can be observed clearly from PANI-b (magnification 2000 ×) and PANI-c (magnification 5000 ×). After electrochemically prepared and assembled on the PANI membrane, the GO layer was manifested on the PANI membrane surface (GO/S-PANI-a). The 2000 × magnified image (GO/S-PANI-b) showed that the GO in flake form completely covered the membrane surface. The oblique stacking of GO sheets can be observed clearly from the 5000 × magnified image (GO/S-PANI-c), providing a favorable spatial structure layer with a thickness of 182 nm (Fig. S6) for water penetration and rejection enhancement of contaminant.

The EDX analysis of GO/S-PANI membrane (GO/S-PANI-d) helps to track the distribution of GO. The mass percentages (wt%) of C and N elements obtained at line data 1, line data 2, and line data 3 (GO/S-PANI-d) were summarized in Table 1. The acquired data for the membrane surface (Line data 1) is of the highest carbon-nitrogen (C/N) ratio of 8.3, achieving a higher value than the pure PANI of 5.0, further reflecting the uniform coverage of the GO layer on the membrane surface. The C/N ratios measured by line data 2 and line data 3 were 5.6 and 5.2, respectively, also confirmed that GO got partially into the finger-like pore layer of the PANI membrane, which benefits the tight binding of the GO layer with the PANI membrane.

Surface roughness is crucial in controlling membrane fouling mitigation, and it can be provided by AFM characterization. As illustrated in Fig. 5, significant differences existed in the 3D AFM images of the PANI and GO/S-PANI membranes. For PANI membrane, a uniform ridge-and-valley morphology could be seen (Fig. 5a), and it was the typical pattern of PANI membrane fabricated by the NIPS method [18]; its root-mean-square roughness (rms) and the average roughness (Ra) were ~ 31.3 nm and ~ 27.8 nm, respectively. When GO was combined with the PANI membrane, a rugged ridge-and-valley morphology for GO/S-PANI membrane (Fig. 5b) appeared, and the rms roughness and the Ra roughness were increased to ~ 47.5 nm and ~ 40.2 nm, respectively. In the cross-flow mode, protein pollution tends to deposit on hydrophobic surfaces and results in reduced membrane reversibility, thus great hydrophilicity can help to alleviate membrane fouling [66]. As confirmed by the Wenzel relation [67], roughness can enhance wettability that a hydrophilic solid ($\theta < 90°$) turns into more hydrophilic when rough. Therefore, the hydrophilicity can be improved after the

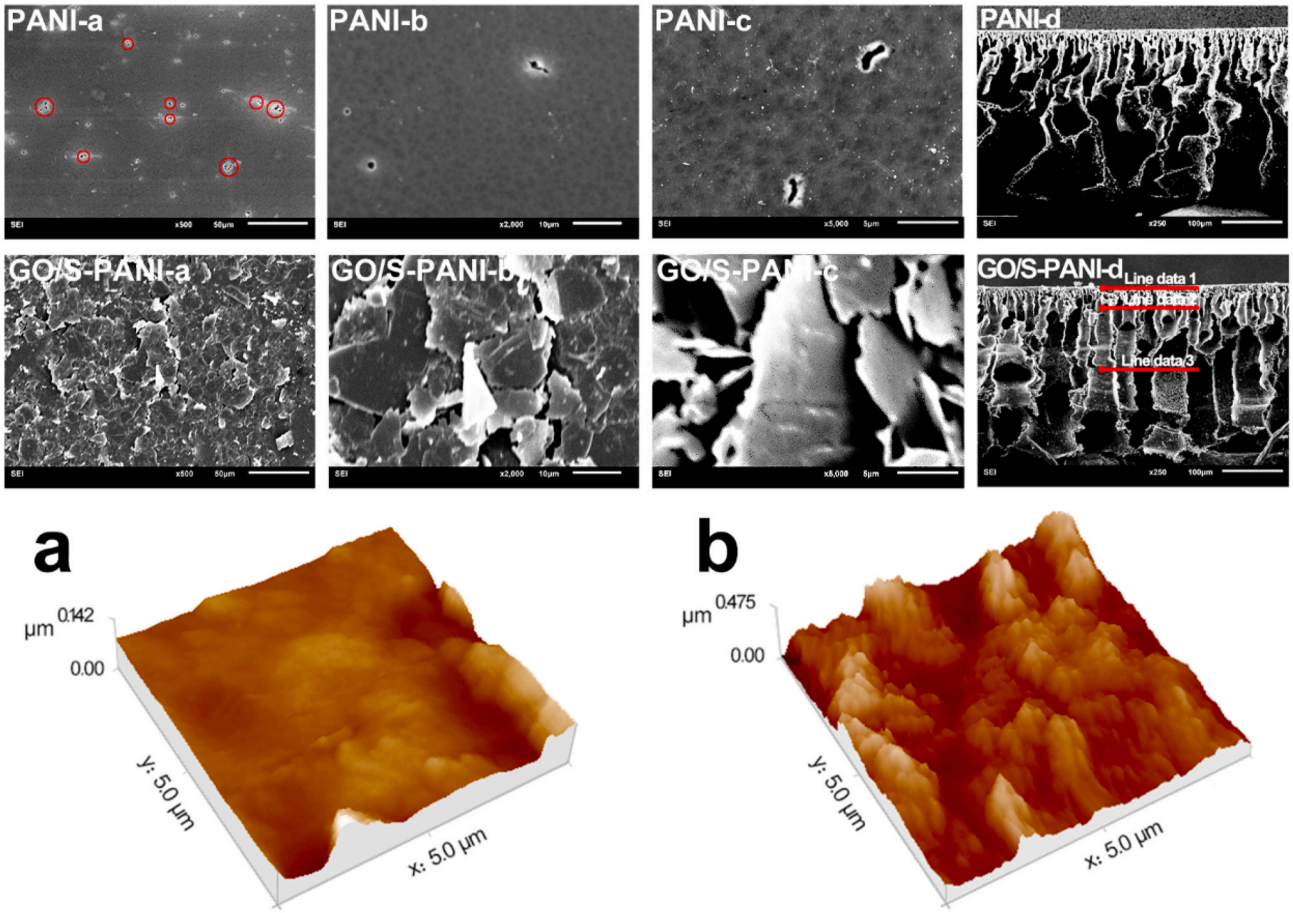

Fig. 5. SEM images of the PANI and GO/S-PANI membranes: top surface magnification 500 × (a), 2000 × (b), 5000 × (c), and cross-section magnification 250 × (d). EDX spectrum analysis: surface layer (Line data 1), finger-like pore up-layer (Line data 2), finger-like pore sub-layer (Line data 3). 3D AFM images of the membranes: PANI membrane (a), GO/S-PANI membrane (b).

Table 1
Membrane cross-sectional EDX spectrum line scanning data.

Mass percentage	Pure PANI	GO/S-PANI		
Position	Sample	Line data 1	Line data 2	Line data 3
C (wt%)	83.2	89.2	84.9	83.9
N (wt%)	16.8	10.8	15.1	16.1
C/N ratio	5.0	8.3	5.6	5.2

PANI membrane ($\theta = 75.9°$) was utilized to prepare the GO/S-PANI membrane, as the rugged ridge-and-valley morphology on GO/S-PANI can enhance the membrane surface roughness. Moreover, the rugged ridge-and-valley morphology can generate local agitation during cross-flow filtration, further limiting blockage and increasing the flux by creating instability [68].

3.1.3. Membrane properties

The tensile strength and elongation at break of the PANI and GO/S-PANI membranes were shown in Fig. 6a. Compared to the PANI membrane, a slight decrease in mechanical strength for the GO/S-PANI membrane was caused by the acid doping in the electrochemical process, which was confirmed by Xu et al. [69] that acid doping could affect the intermolecular reconfiguration of the PANI backbone, causing the reduction in membrane strength. The PANI membrane, which was only immersed in sulfuric acid (1.1 mol/L) for 2 h, was named the S-PANI membrane and was also tested as a comparison (Fig. S7). The obtained results for the tensile strength and elongation at break were lower than that of the GO/S-PANI membrane, indicating that the composite GO layers can enhance the overall membrane mechanical properties.

Pore size and pore size distribution (PSD) of the PANI and GO/S-PANI membranes were given in Table 2 and Fig. 6b, respectively. As the crack-like pores existed on the PANI membrane surface, a wide pore size distribution ranged from 0.27 μm to 6.11 μm were detected. Nonetheless, the average pore diameter for the PANI membrane was only 1.18 μm. On the other hand, impacted by the combined GO, a constrictive pore size distribution from 0.16 μm to 2.31 μm with an average pore diameter of 0.84 μm was acquired by the GO/S-PANI membrane. Once the GO was assembled on the PANI membrane and formed a layer, the surface crack-like pores were significantly reduced, which improves the membrane rejection of yeast pollutants and brings about a more stable pore structure. Besides, the introduction of GO did not affect porosity, and it only reduced from 82.94% for the PANI membrane to 78.24% for the GO/S-PANI membrane.

Membrane hydrophilicity can be obtained by the dynamic contact angle of water on the membrane. The difference in change of water contact angles with time gives a quantitative indication of the membranes. Based on Fig. 6c, the water contact angle changed from 81.3° to 75.9° for PANI membrane and from 40.2° to 37.1° for GO/S-PANI membrane. The S-PANI membrane was also utilized to study the effect of acid doping on hydrophilicity, and the obtained result was 65.4° at the original time and 60.7° in the end (Fig. S8a). By comparing the final hydrophilicity of the S-PANI membrane (60.7°) and GO/S-PANI membrane (37.1°), a conclusion can be drawn that the GO layer was highly hydrophilic and had a strong impact on the hydrophilicity of the GO/S-PANI membrane. According to AFM, GO layers made the GO/S-PANI membrane surface rougher than that of the PANI membrane, which

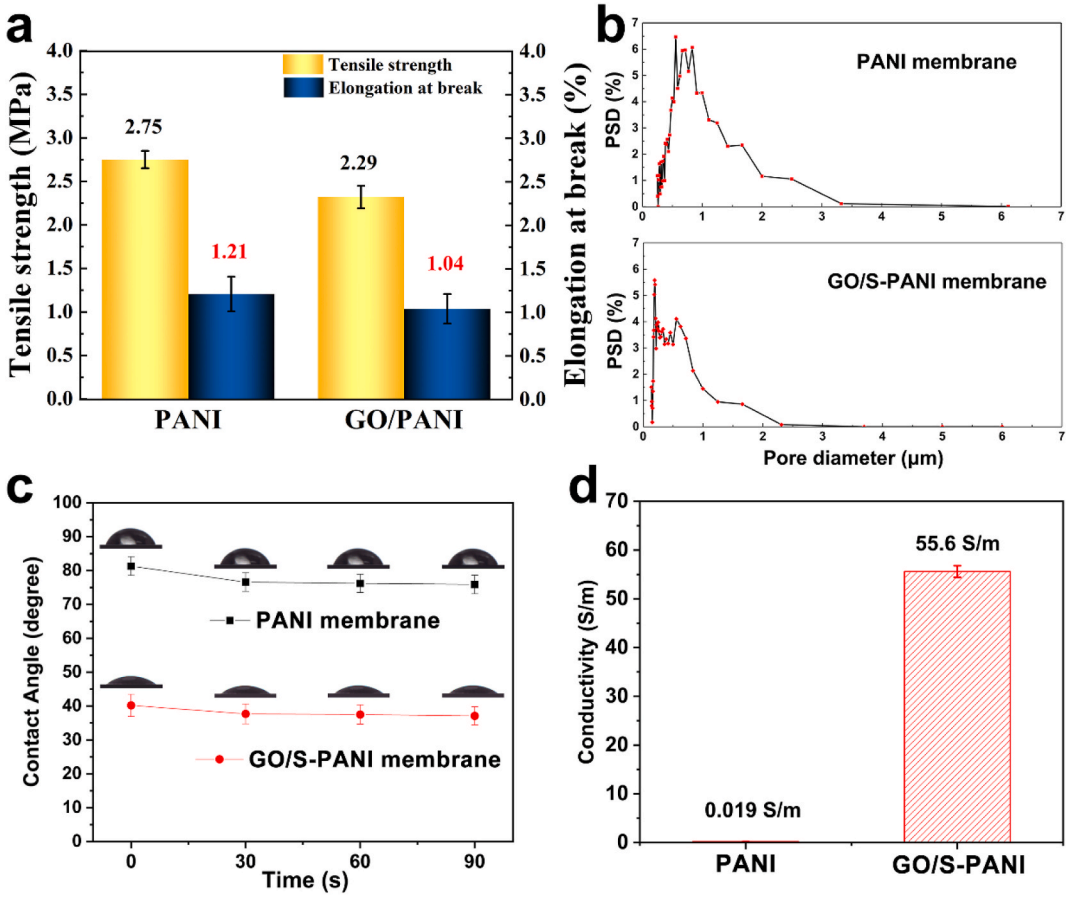

Fig. 6. Properties of PANI and GO/S-PANI membranes: (a) Mechanical properties: Tensile strength and elongation at break (%). (b) Pore size distribution. (c) Dynamic water contact angles. (d) Membrane conductivity.

Table 2
Pore sizes and Porosity of the PANI and GO/S-PANI membranes.

Pore size Membrane	Maximum (μm)	Mean (μm)	Minimum (μm)	Porosity (%)
PANI	6.11 ± 0.21	1.18 ± 0.09	0.27 ± 0.04	82.94 ± 1.73
GO/S-PANI	2.31 ± 0.14	0.84 ± 0.11	0.16 ± 0.07	78.24 ± 2.18

might be another reason for the increase in membrane hydrophilicity.

The conductivities of the membranes wetted with deionized water have been shown in Fig. 6d. The membrane reaching high conductivity was mainly provided by acid doping, and this could be confirmed from the comparison of conductivities: the conductivity was enhanced from 0.019 S m^{-1} for the PANI membrane to 58.1 S m^{-1} for the S-PANI membrane (Fig. S8b), after GO was assembled on the membrane, the conductivity was slightly decreased to 55.6 S m^{-1}.

Cyclic voltammetry (CV) was carried out to determine whether redox reactions occurred on the membrane surface. The CV scan for the GO/S-PANI membrane in Fig. S9a revealed that no redox peak, proving that the electrooxidation did not happen on the membrane surface during electrofiltration. As schemed in Fig. S9b, the obtained surface zeta potential was −35.4 ± 1.4 mV for the PANI membrane and −52.9 ± 5.1 mV for the GO/S-PANI membrane indicating that the GO/S-PANI membrane owned favorable electronegativity which could generate electrostatic repulsion to yeast pollutants (Zeta potential: −12.9 mV).

3.2. Electrofiltration experiment

3.2.1. Effect of different low voltages on water permeability and rejection rate

Contrast experiments for membrane permeability have been explored at low voltages of 1 V, 2 V, and 3 V. Experiments were carried out using 2 g L^{-1} yeast suspension as the feed. From Fig. 7a, for GO/S-PANI membrane under 1 V, 2 V, and 3 V, the average permeation fluxes were 190.16 L m^{-2} h^{-1}, 194.78 L m^{-2} h^{-1}, and 203.06 L m^{-2} h^{-1}, which were higher than obtained without voltages applied (68.37 L m^{-2} h^{-1}). The rejection rate is also an important index to the membrane performance and is summarized in Fig. 7b. Due to the deformation under pressure filtration, yeast pollutants can pass through the membrane pores which were smaller than themselves. For the PANI membrane, resulting from the existence of crack-like pores on the membrane surface, the rejection rates of yeast particles were only 70.4% under 0 V and 75.2% under 1 V. For GO/S-PANI membrane, the rejection rates had been significantly improved to 87.5% when no voltage applied, and slightly increased to 90.2%, 92.0%, and 93.1% under 1 V, 2 V, and 3 V respectively, indicating that the electrochemically designed GO layer can enhance membrane rejection for yeasts.

3.2.2. Effect of applied and unapplied low voltage on water permeability

Considering the requirements of rejection and energy-efficient, water permeability under 1 V applied or 0 V was depicted in Figs. 7c-f. As observed in Fig. 7c, semi-conducting PANI membrane limited its use in electrofiltration, resulting in insignificant changes. The total permeation flux for 1 V applied was only 1.10 times of those without voltage. Besides, for the tests without and with 1 V applied, the lowest fluxes in the third cycle were 7.81 L m^{-2} h^{-1} and 12.33 L m^{-2} h^{-1},

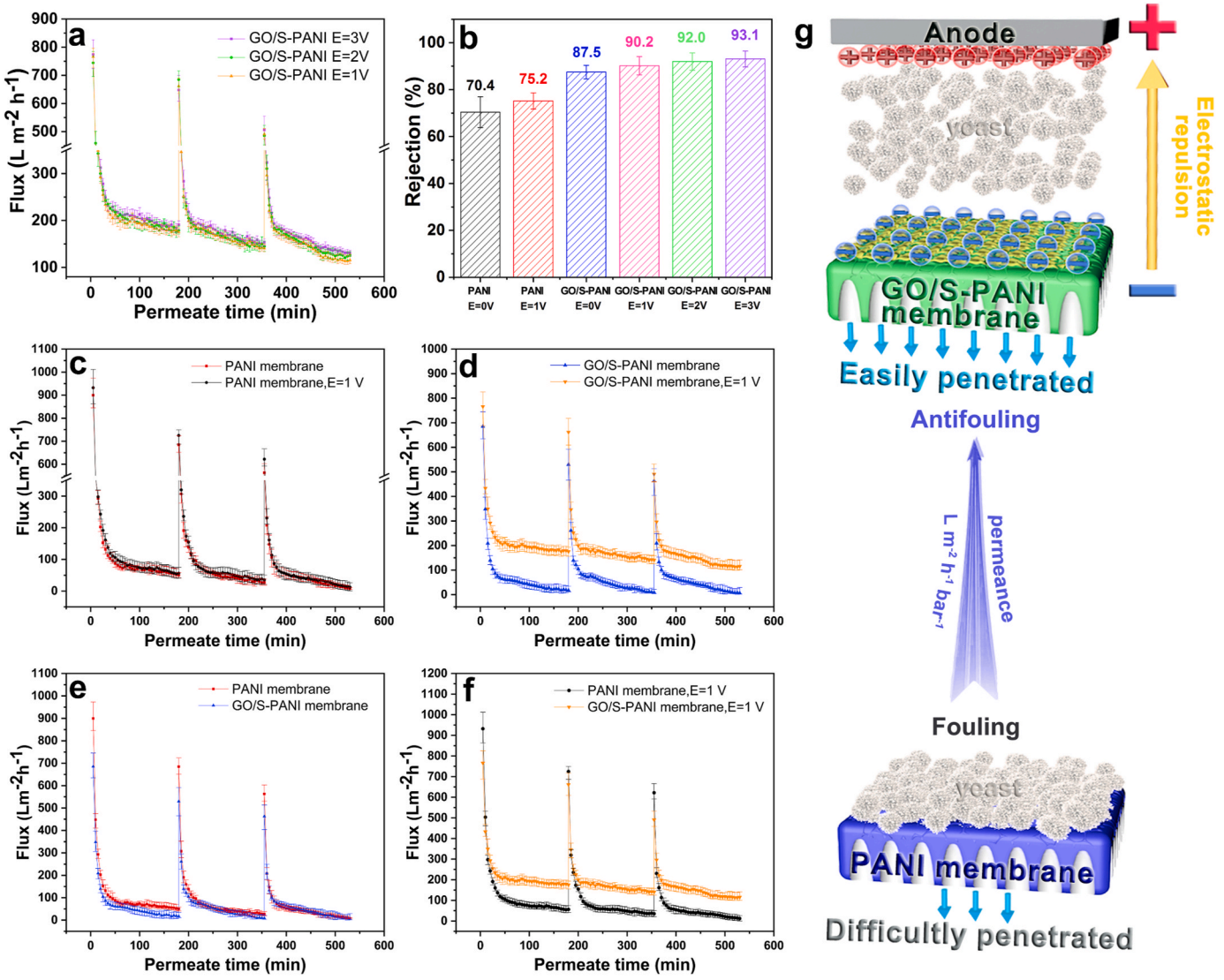

Fig. 7. (a) Variation of permeation flux of GO/S-PANI membrane in three cycles under applied 1 V, 2 V, and 3 V, respectively. (b) The rejection rate of membranes under applied different electric fields. (c–f) Variation of permeation flux of PANI and GO/S-PANI membranes, with 0 V or 1 V applied in three cycles. (g) Schematic illustration of electrical repulsion and water permeability enhancement.

respectively. Membrane permeability decreased with the clogging of the yeasts to the membranes over time. Consequently, poor membrane conductivity led to the unpractical efficacy of the electrofiltration. While the GO/S-PANI membrane showed better results as presented in Fig. 7d. The average flux increased greatly from 68.37 L m^{-2} h^{-1} without electric field to 190.16 L m^{-2} h^{-1} with 1 V. It could still reach 115.41 L m^{-2} h^{-1} at the end of the third cycle, indicating the enhancement of membrane permeability during the electrofiltration process.

As shown in Fig. 7e, the downtrend was analogous without electric fields for both membranes. Although the crack-like pores and the relatively higher porosity could be helpful to gain a greater flux for the PANI membrane, the rejection rate obtained was only 70.4%. Better hydrophilicity and larger electronegativity for the GO/S-PANI membrane could enhance its resistance to yeast pollutants, impelling the permeation flux of the GO/S-PANI membrane to maintain relative stability. Also, benefit from GO layers, the rejection rate could reach 87.5%.

Fig. 7f contrasted the flux curves under 1 V for the PANI membrane and GO/S-PANI membrane. The average permeation flux of the GO/S-PANI membrane was 1.97 times that of the PANI membrane. Compared to the PANI membrane with a q value of 38.85%, the permeability for the GO/S-PANI membrane gained a q value of 177.01%. As observed through the q value of each cycle in Table 3, the permeation stability for the GO/S-PANI membrane demonstrated better results.

3.2.3. *Effect of GO layer on GO/S-PANI membrane*

The S-PANI membrane was also tested to filter 2 g L^{-1} yeast suspension as a comparison. For the S-PANI membrane and GO/S-PANI membrane, an inconspicuous difference was displayed between their permeation fluxes (Fig. 8a). However, the rejection rates were significantly different (Fig. 8c). The rejection rate for the GO/S-PANI membrane was 87.5%, and it was 72.9% for the S-PANI membrane, proving the improvement in the rejection rate by the formed GO layer on the

Table 3
The increased rate of total permeation flux (q) for membranes.

Membrane sample	1st cycle	2nd cycle	3rd cycle	Average
GO/S-PANI membrane	191.07% ± 14.12%	176.66% ± 18.24%	163.30% ± 12.27%	177.01% ± 14.87%
PANI membrane	69.38% ± 11.65%	38.11% ± 12.72%	9.05% ± 7.94%	38.85% ± 10.77%

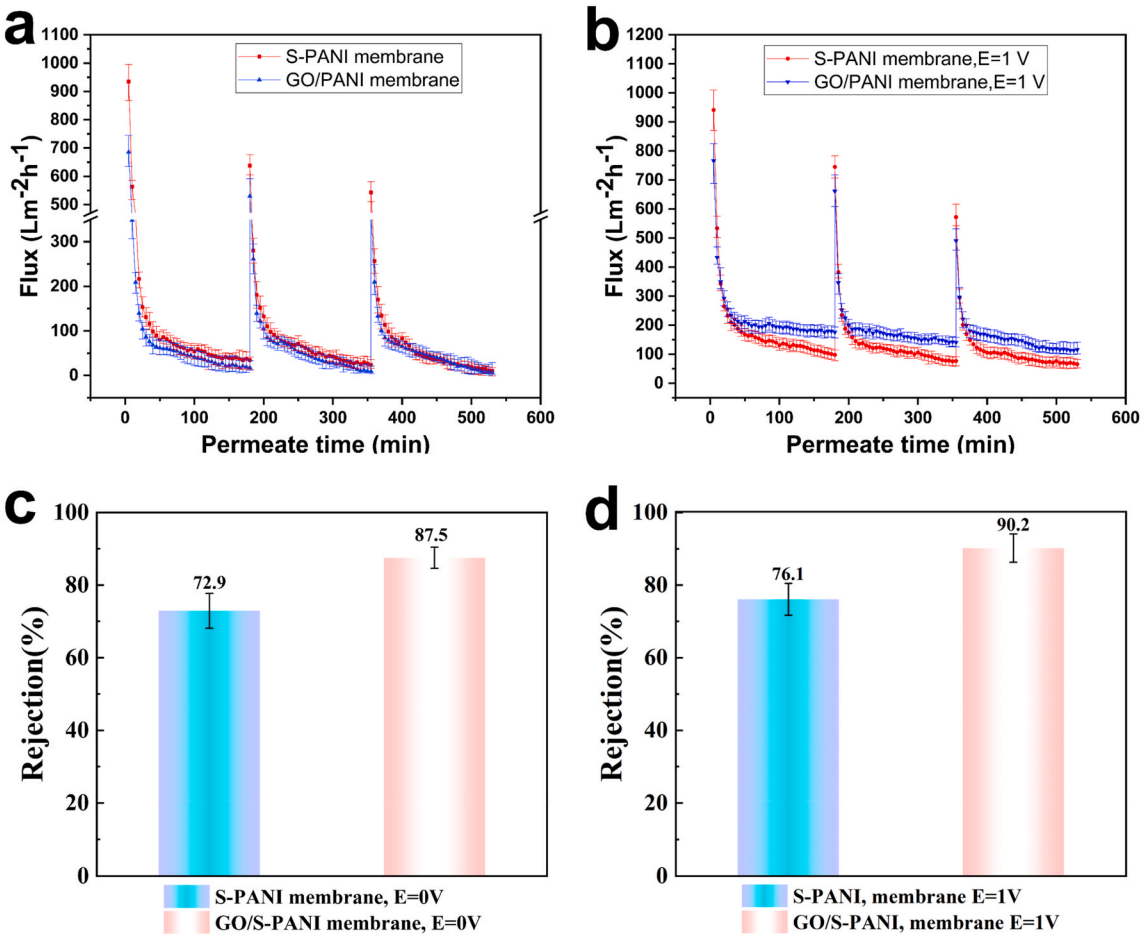

Fig. 8. (a) Variation of permeation flux of S-PANI and GO/S-PANI membranes under 0 V. (b) Variation of permeation flux of S-PANI and GO/S-PANI membranes under 1 V. (c) The rejection rate of membranes under 0 V. (d) The rejection rate of membranes under 1 V.

GO/S-PANI membrane.

According to Fig. 8b, by adjusting the source to 1 V, the permeation flux of the GO/S-PANI membrane was 1.30 times that of the S-PANI membrane. The results can be attributed to two aspects: (1) the hydrophilic groups on GO allowed water molecules to embed the GO interlayer structure quickly [70]; (2) the generated electrostatic repulsion assisted in alleviating pollution [5]. With 1 V applied (Fig. 8d), the rejection rate for the S-PANI membrane was only 76.1% and could still be around 90.2% for the GO/S-PANI membrane, indicating the stable rejection rate for the GO/S-PANI membrane. Compared to the S-PANI membrane, the GO/S-PANI membrane displayed greater appositeness towards electrofiltration and showed improved performance.

3.2.4. *Description of factors influencing and controlling water permeability*

Since the CV scan showed no redox peaks, it suggested that the electrooxidation did not occurred while the electrical repulsion played a decisive role in the electrofiltration process. During this process, the membrane surface exhibited negatively charged when the cathode conductor was powered up. Thus, the electrostatic repulsive force was generated between membrane surface and yeast pollutants, resulting in less readily adsorbed/remained yeasts on the membrane surface, the permeation flux was enhanced (Fig. 7g). Moreover, the GO layer was full of hydrophilic hydroxyl and carboxyl groups, forming nanochannels between the GO sheets and allowing water molecules to pass through them quickly [14,23]. According to the literature [40], the stacking method of adjacent GO sheets affects the interlayer nanostructure, which can control water transport among neighboring GO layers. The larger the interlayer spacing is, the more water permeation channels are generated; the wider the channel is, the larger the volume for the containment of water molecules is. The great volume can weaken the viscous interfacial resistance to water transport. In our electrochemical strategy, the GO sheets in membrane fabrication were self-assembled, making GO sheets stacked in the loosest manner of the three ways (i.e., oxygen-containing groups face to face, pristine graphene facing each other, and oxygen-containing groups face to pristine graphene [40]). The interlayer structure of GO layers was mainly determined by the existing oxygen-containing groups, and this stacking way could form expanded layer spacing and more significant volume nanochannels. Also, these hydrophilic groups on GO allowed water molecules to embed the GO interlayer structure quickly, and water molecules could go through GO by taking a flexuous pathway inside the vacant space of oxidized regions within GO sheets [70,71]. Besides, the GO layer induced an increase in the electronegativity of the membrane surface, thereby enhancing the electrostatic repulsion to yeasts. Based on the above conditions, the as-prepared GO/S-PANI membrane presented a good water permeability and contaminant rejection.

3.2.5. *Stability of GO/S-PANI membrane*

The GO/S-PANI membranes were achieved after electrofiltration tests under 0 V and 1 V, and membrane stability was investigated from four aspects: SEM image, water contact angle, pore size, and conductivity. Compared with at 1 V (Fig. 9b), the GO/S-PANI membrane at 0 V (Fig. 9a) showed more distinct yeast aggregates (green circles). Besides, GO sheets were partially lost at 0 V, leading to the appearance of crack-like holes (red circles). The above conclusions were also confirmed by membrane hydrophilicity (Fig. 9c) and membrane pore sizes (Fig. 9d);

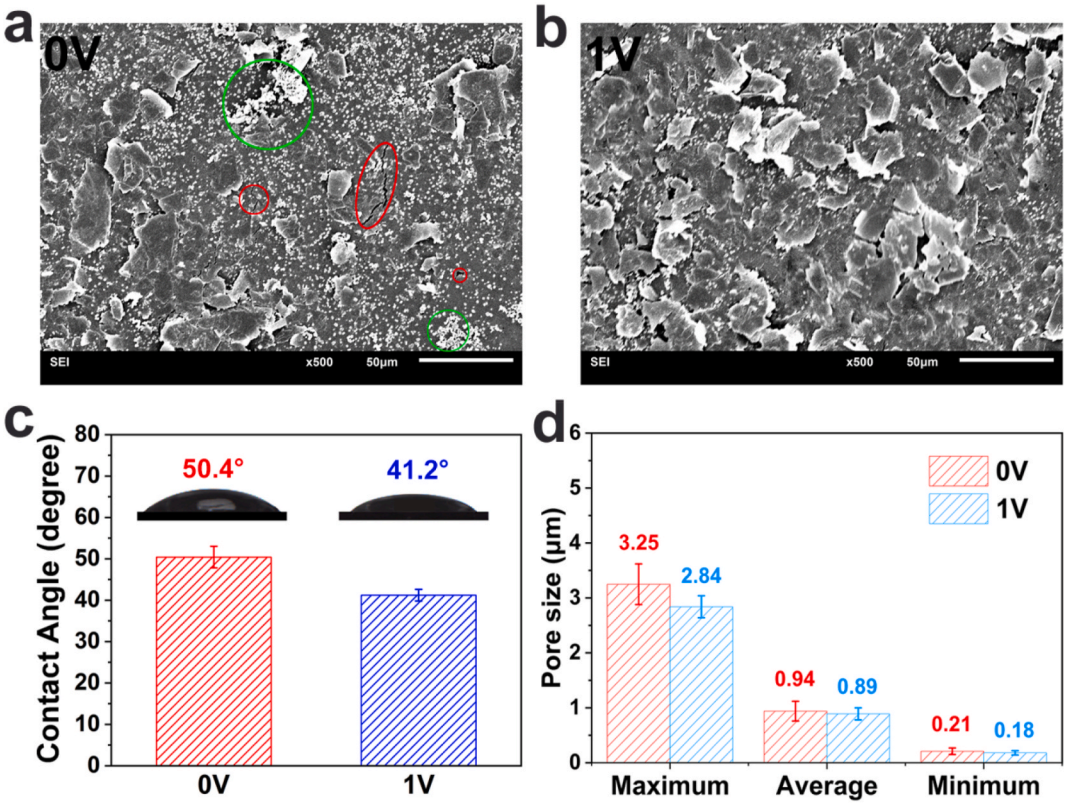

Fig. 9. (a) SEM image of the GO/S-PANI membrane magnification 500 × after tests under 0 V. (b) SEM image of the GO/S-PANI membrane magnification 500 × after tests under 1 V. (c) Water contact angles of the GO/S-PANI membrane after tests under 0 V and 1 V. (d) Pore sizes of the GO/S-PANI membrane after tests under 0 V and 1 V.

both values increased compared with the original membrane. The water contact angle for 1 V was 41.2° and was 50.4° for 0 V; meanwhile, the pore size (Maximum) showed 2.84 μm and 3.25 μm respectively, suggesting the membrane was relatively stable at 1 V. To verify the possible acid leaching from the membrane, the conductivities of the GO/S-PANI membrane were tested after each cycle (Fig. S10). Reduced conductivities were observed at both 0 V and 1 V with the increase of cycle numbers, indicating acid leaching occurred during the electrofiltration processes. Membrane conductivities decreased more when at 0 V than at 1 V, reflecting that the conductive stability for the GO/S-PANI membrane was better with the utilization of voltage.

The GO/S-PANI membrane, with rugged ridge-and-valley morphology (Fig. 5), was conducive to the formation of local agitation, which could reduce the adsorption potential of yeasts [68]. However, as the test time progressed, larger yeast particles (green circles in Fig. 9a, Fig. S4) could be formed through the agglomeration of yeast particles in the feed, which made an increased affinity of yeasts to adsorb the GO sheets on the membrane. Acted by the tangential force of water flow, the yeast-adhered GO sheets were partly lost from the membrane surface. In the absence of electric fields, membrane hydrophilicity and electrostatic repulsion can partially mitigate yeast adsorption. While as the gradual increase in the loss of GO sheets, above membrane properties weakened, resulting in membrane fouling and stability decreasing. Under the electric field, the continuous electric repulsion greatly reduced yeast adsorption. The added copper ions also stabilized the GO layers [45], contributing to GO layers being more stable.

3.3. Antibacterial activity of membrane

The antibacterial ability of membranes was tested using Escherichia coli (E. Coli). As shown in Fig. 10, compared with the control plate, the number of E. coli colonies on the plate treated by the PANI membrane displayed no distinct changes. However, the plate treated by GO/S-PANI

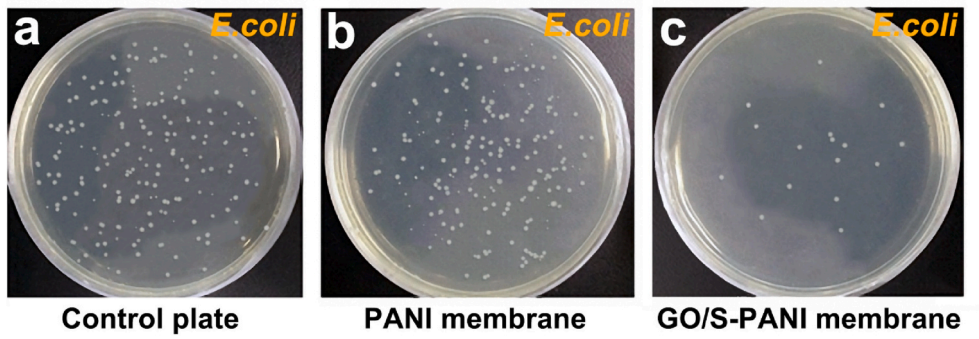

Fig. 10. Photographs of E. coli colonies on the agar plate: the control plate (a), PANI membrane (b), and GO/S-PANI membrane (c).

membrane was significantly decreased, indicating antibacterial ability was enhanced by the GO/S-PANI membrane. The antibacterial rate could be used to analyze the antibacterial activity of membranes quantitatively. The rate reached 92.1% for the GO/S-PANI membrane, which implied that the membrane had excellent antibacterial ability.

The mechanism of antibacterial activity of the GO/S-PANI membrane could be explained as follows: (1) After the direct contact with GO sheets, the destruction of cell structures could happen due to the shear stress of GO sheets, leading to irreversible damage of bacterial cells [24]. (2) As the electrostatic adherence between Cu^{2+} and negatively charged bacteria, the bacteria wall might be destroyed and leaked out the contents in bacteria, which finally led the bacteria to die, thereby the formed GO/Cu^{2+} on the GO/S-PANI membrane could greatly increase the antibacterial activity than that of the pure GO [46,72]. (3) As the GO/S-PANI membrane was doped by sulfuric acid, the acid dopant on the PANI chains could contact the E. Coli, resulting in bacterial death [73]. Overall, the GO/S-PANI membrane can be considered as a potential material for antibacterial.

4. Conclusion

Through electrochemical strategy, the graphene oxide/sulfuric acid doped polyaniline (GO/S-PANI) membrane was readily fabricated. Copper ions were both the driving agent for electrochemical membrane-formation and the stabilizer for GO layers. The conductivity of the GO/S-PANI membrane (55.6 S m^{-1}) was three orders of magnitude higher than that of the PANI membrane (0.019 S m^{-1}). Affected by the hydrophilic GO layer, the GO/S-PANI membrane became highly hydrophilic with a water contact angle of 37.1°. The surface zeta potential decreased from −35.4 ± 1.4 mV (PANI membrane) to −52.9 ± 5.1 mV (GO/S-PANI membrane), providing an increased membrane resistance to negatively charged yeasts (Zeta potential: −12.9 mV). The pore structure of the developed membrane was more favorable for rejecting yeast pollutants (2–5 μm). Under low-intensity electric fields, the GO/S-PANI membrane showed better antifouling performance and preferable water permeability than the PANI membrane. For the electrofiltration process, the GO/S-PANI membrane demonstrated greater stability than without electric fields. The improved antibacterial rate was shown by the GO/S-PANI membrane, which can be against E. Coli up to 92.1%. This study provides a strategy for facile preparation of the GO/S-PANI conductive membrane with application potential in electrofiltration and antibacterial fields.

CRediT authorship contribution statement

Bojun Li: Conceptualization, Methodology, Formal analysis, Visualization, Investigation, Writing – original draft. **Wenjing Tang:** Investigation, Formal analysis, Validation, Software. **De Sun:** Project administration, Conceptualization, Funding acquisition, Resources. **Bingbing Li:** Supervision, Writing – review & editing. **Yanxia Ge:** Validation. **Xin Ye:** Software. **Wei Fang:** Visualization.

Declaration of competing interest

The authors declared that they have no conflicts of interest to this work.

We declare that we do not have any commercial or associative interest that represents a conflict of interest in connection with the work submitted.

Acknowledgment

This work was supported by the Chinese National Key R&D Plan [grant numbers 2018YFB0504600, 2018YFB0504603]; the Foundation of Jilin Educational Committee, Jilin, China [grant number JJKH20191318KJ].

Appendix A. Supplementary data

Supplementary data to this article can be found online at https://doi.org/10.1016/j.memsci.2021.119844.

References

[1] M.A. Shannon, P.W. Bohn, M. Elimelech, J.G. Georgiadis, B.J. Mariñas, A. M. Mayes, Science and technology for water purification in the coming decades, Nature 452 (2008) 301–310.
[2] H.-C. Flemming, Microbial biofouling: unsolved problems, insufficient approaches, and possible solutions, in: Biofilm Highlights, Springer, 2011, pp. 81–109.
[3] A. Ronen, W. Duan, I. Wheeldon, S.L. Walker, D. Jassby, Microbial attachment inhibition through low voltage electrochemical reactions on electrically conducting membranes, Environ. Sci. Technol. 49 (2015) 12741–12750.
[4] G. Chen, Electrochemical technologies in wastewater treatment, Separ. Purif. Technol. 38 (2004) 11–41.
[5] P. Formoso, E. Pantuso, G. Filpo, F. Nicoletta, Electro-conductive membranes for permeation enhancement and fouling mitigation: a short review, Membranes 7 (2017) 39.
[6] M. Sun, X. Wang, L.R. Winter, Y. Zhao, W. Ma, T. Hedtke, J.-H. Kim, M. Elimelech, Electrified Membranes for Water Treatment Applications, ACS ES&T Engineering, 2021.
[7] J. Sun, C. Hu, B. Wu, J. Qu, Fouling mitigation of a graphene hydrogel membrane electrode by electrical repulsion and in situ self-cleaning in an electro-membrane reactor, Chem. Eng. J. 393 (2020) 124817.
[8] L. Liu, F. Zhao, J. Liu, F. Yang, Preparation of highly conductive cathodic membrane with graphene (oxide)/PPy and the membrane antifouling property in filtrating yeast suspensions in EMBR, J. Membr. Sci. 437 (2013) 99–107.
[9] B.P. Chaplin, The prospect of electrochemical technologies advancing worldwide water treatment, Acc. Chem. Res. 52 (2019) 596–604.
[10] C. Thamaraiselvan, A. Ronen, S. Lerman, M. Balaish, Y. Ein-Eli, C.G. Dosoretz, Low voltage electric potential as a driving force to hinder biofouling in self-supporting carbon nanotube membranes, Water Res. 129 (2018) 143–153.
[11] T.X. Huong Le, L.F. Dumée, S. Lacour, M. Rivallin, Z. Yi, L. Kong, M. Bechelany, M. Cretin, Hybrid graphene-decorated metal hollow fibre membrane reactors for efficient electro-Fenton - filtration co-processes, J. Membr. Sci. 587 (2019) 117182.
[12] K. Wang, L. Xu, K. Li, L. Liu, Y. Zhang, J. Wang, Development of polyaniline conductive membrane for electrically enhanced membrane fouling mitigation, J. Membr. Sci. 570–571 (2019) 371–379.
[13] L. Liu, J. Liu, B. Gao, F. Yang, S. Chellam, Fouling reductions in a membrane bioreactor using an intermittent electric field and cathodic membrane modified by vapor phase polymerized pyrrole, J. Membr. Sci. 394–395 (2012) 202–208.
[14] K.G. Zhou, K.S. Vasu, C.T. Cherian, M. Neek-Amal, J.C. Zhang, H. Ghorbanfekr-Kalashami, K. Huang, O.P. Marshall, V.G. Kravets, J. Abraham, Y. Su, A. N. Grigorenko, A. Pratt, A.K. Geim, F.M. Peeters, K.S. Novoselov, R.R. Nair, Electrically controlled water permeation through graphene oxide membranes, Nature 559 (2018) 236–240.
[15] Q. Zhang, P. Arribas, E.M. Remillard, M.C. García-Payo, M. Khayet, C.D. Vecitis, Interlaced CNT electrodes for bacterial fouling reduction of microfiltration membranes, Environ. Sci. Technol. 51 (2017) 9176–9183.
[16] N. Li, L. Liu, F. Yang, Highly conductive graphene/PANi-phytic acid modified cathodic filter membrane and its antifouling property in EMBR in neutral conditions, Desalination 338 (2014) 10–16.
[17] A. Ronen, S.L. Walker, D. Jassby, Electroconductive and electroresponsive membranes for water treatment, Rev. Chem. Eng. 32 (2016) 533–550.
[18] A. Sarihan, S. Shahid, J. Shen, I. Amura, D.A. Patterson, E.A.C. Emanuelsson, Exploiting the electrical conductivity of poly-acid doped polyaniline membranes with enhanced durability for organic solvent nanofiltration, J. Membr. Sci. 579 (2019) 11–21.
[19] E.L. Subtil, J. Gonçalves, H.G. Lemos, E.C. Venancio, J.C. Mierzwa, J. dos Santos de Souza, W. Alves, P. Le-Clech, Preparation and characterization of a new composite conductive polyethersulfone membrane using polyaniline (PANI) and reduced graphene oxide (rGO), Chem. Eng. J. 390 (2020) 124612.
[20] L.L. Xu, S. Shahid, D.A. Patterson, E.A.C. Emanuelsson, Flexible electro-responsive in-situ polymer acid doped polyaniline membranes for permeation enhancement and membrane fouling removal, J. Membr. Sci. 578 (2019) 263–272.
[21] I.F. Amura, S. Shahid, A. Sarihan, J. Shen, D.A. Patterson, E.A.C. Emanuelsson, Fabrication of self-doped sulfonated polyaniline membranes with enhanced antifouling ability and improved solvent resistance, J. Membr. Sci. 620 (2021) 117712.
[22] H. Alhweij, E.A.C. Emanuelsson, S. Shahid, J. Wenk, Simplified in-situ tailoring of cross-linked self-doped sulfonated polyaniline (S-PANI) membranes for nanofiltration applications, J. Membr. Sci. 637 (2021) 119654.
[23] H. Wang, W. Wang, L. Wang, B. Zhao, Z. Zhang, X. Xia, H. Yang, Y. Xue, N. Chang, Enhancement of hydrophilicity and the resistance for irreversible fouling of polysulfone (PSF) membrane immobilized with graphene oxide (GO) through chloromethylated and quaternized reaction, Chem. Eng. J. 334 (2018) 2068–2078.
[24] S. Liu, T.H. Zeng, M. Hofmann, E. Burcombe, J. Wei, R. Jiang, J. Kong, Y. Chen, Antibacterial activity of graphite, graphite oxide, graphene oxide, and reduced graphene oxide: membrane and oxidative stress, ACS Nano 5 (2011) 6971–6980.
[25] B. Shi, H. Wu, J. Shen, L. Cao, X. He, Y. Ma, Y. Li, J. Li, M. Xu, X. Mao, M. Qiu, H. Geng, P. Yang, Z. Jiang, Control of edge/in-plane interactions toward robust,

highly proton conductive graphene oxide membranes, ACS Nano 13 (2019) 10366–10375.
[26] L. Chen, G. Shi, J. Shen, B. Peng, B. Zhang, Y. Wang, F. Bian, J. Wang, D. Li, Z. Qian, G. Xu, G. Liu, J. Zeng, L. Zhang, Y. Yang, G. Zhou, M. Wu, W. Jin, J. Li, H. Fang, Ion sieving in graphene oxide membranes via cationic control of interlayer spacing, Nature 550 (2017) 380–383.
[27] L. Jianhua, A. Junwei, Z. Yecheng, M. Yuxiao, L. Mengliu, Y. Mei, L. Songmei, Preparation of an amide group-connected graphene–polyaniline nanofiber hybrid and its application in supercapacitors, ACS Appl. Mater. Interfaces 4 (2012) 2870–2876.
[28] R.-X. Wang, L.-F. Huang, X.-Y. Tian, Understanding the protonation of polyaniline and polyaniline–graphene interaction, J. Phys. Chem. C 116 (2012) 13120–13126.
[29] Q. Zhang, Y. Li, Y. Feng, W. Feng, Electropolymerization of graphene oxide/polyaniline composite for high-performance supercapacitor, Electrochim. Acta 90 (2013) 95–100.
[30] T. Rezazadeh, N. Dalali, N. Sehati, Investigation of adsorption performance of graphene oxide/polyaniline reinforced hollow fiber membrane for preconcentration of Ivermectin in some environmental samples, Spectrochim. Acta A 204 (2018) 409–415.
[31] H. Kweon, C.-W. Lin, M.M. Faruque Hasan, R. Kaner, G.N. Sant, Highly permeable polyaniline–graphene oxide nanocomposite membranes for CO2 separations, ACS Appl. Polym. Mater 1 (2019) 3233–3241.
[32] V. Shalini, M. Navaneethan, S. Harish, J. Archana, S. Ponnusamy, H. Ikeda, Y. Hayakawa, Design and fabrication of PANI/GO nanocomposite for enhanced room-temperature thermoelectric application, Appl. Surf. Sci. 493 (2019) 1350–1360.
[33] W. Jr, R. Offeman, Preparation of graphitic oxide, J. Am. Chem. Soc. 80 (1958).
[34] R. Muzyka, M. Kwoka, Ł. Smędowski, N. Díez, G. Gryglewicz, Oxidation of graphite by different modified Hummers methods, N. Carbon Mater. 32 (2017) 15–20.
[35] S. Lee, J. Oh, R.S. Ruoff, S. Park, Residual acetone produces explosives during the production of graphite oxide, Carbon 50 (2012) 1442–1444.
[36] J. Cao, P. He, M.A. Mohammed, X. Zhao, R.J. Young, B. Derby, I.A. Kinloch, R.A. W. Dryfe, Two-step electrochemical intercalation and oxidation of graphite for the mass production of graphene oxide, J. Am. Chem. Soc. 139 (2017) 17446–17456.
[37] S. Pei, Q. Wei, K. Huang, H.-M. Cheng, W. Ren, Green synthesis of graphene oxide by seconds timescale water electrolytic oxidation, Nat. Commun. 9 (2018).
[38] S. Fang, Y. Lin, Y.H. Hu, Recent advances in green, safe, and fast production of graphene oxide via electrochemical approaches, ACS Sustain. Chem. Eng. 7 (2019) 12671–12681.
[39] B. Mi, Graphene oxide membranes for ionic and molecular sieving, Science 343 (2014) 740.
[40] W. Li, L. Zhang, X. Zhang, M. Zhang, T. Liu, S. Chen, Atomic insight into water and ion transport in 2D interlayer nanochannels of graphene oxide membranes: implication for desalination, J. Membr. Sci. 596 (2020) 117744.
[41] B. Li, D. Sun, B. Li, W. Tang, P. Ren, J. Yu, J. Zhang, One-step electrochemically prepared graphene/polyaniline conductive filter membrane for permeation enhancement by fouling mitigation, Langmuir 36 (2020) 2209–2222.
[42] Y. Roichman, G.I. Titelman, M.S. Silverstein, A. Siegmann, M. Narkis, Polyaniline synthesis: influence of powder morphology on conductivity of solution cast blends with polystyrene, Synth. Met. 98 (1999) 201–209.
[43] S.M. Krishna, S. Cheunkar, B. Lertanantawong, R. Thippeswamy, N. D H, W. Surareungchai, B. Geetha, K. Reddy, Graphene oxide-Cu (II) composite electrode for non-enzymatic determination of hydrogen peroxide, J. Electroanal. Chem. (2016) 776.
[44] K. Yang, B. Chen, X. Zhu, B. Xing, Aggregation, adsorption, and morphological transformation of graphene oxide in aqueous solutions containing different metal cations, Environ. Sci. Technol. 50 (2016) 11066–11075.
[45] X.-B. Lv, R. Xie, J.-Y. Ji, Z. Liu, X.-Y. Wen, L.-Y. Liu, J.-Q. Hu, X.-J. Ju, W. Wang, L.-Y. Chu, A novel strategy to fabricate cation-cross-linked graphene oxide membrane with high aqueous stability and high separation performance, ACS Appl. Mater. Interfaces 12 (2020) 56269–56280.
[46] S. Zavareh, E. Norouzi, Impregnation of GO with Cu2+ for enhancement of aniline adsorption and antibacterial activity, J. Water Process Eng. 20 (2017) 160–167.
[47] M. Chandler, A. Zydney, Effects of membrane pore geometry on fouling behavior during yeast cell microfiltration, J. Membr. Sci. 285 (2006) 334–342.
[48] M. Ramezanzadeh, M. Asghari, B. Ramezanzadeh, G. Bahlakeh, Fabrication of an efficient system for Zn ions removal from industrial wastewater based on graphene oxide nanosheets decorated with highly crystalline polyaniline nanofibers (GO-PANI): Experimental and ab initio quantum mechanics approaches, Chem. Eng. J. 337 (2018) 385–397.
[49] S. Eigler, S. Grimm, F. Hof, A. Hirsch, Graphene oxide: a stable carbon framework for functionalization, J. Mater. Chem. A 1 (2013) 11559–11562.
[50] J. Tang, X. Jing, B. Wang, F. Wang, Infrared spectra of soluble polyaniline, Synth. Met. 24 (1988) 231–238.
[51] G. Wang, W. Xing, S. Zhuo, The production of polyaniline/graphene hybrids for use as a counter electrode in dye-sensitized solar cells, Electrochim. Acta 66 (2012) 151–157.
[52] I. Šeděnková, M. Trchová, J. Stejskal, Thermal degradation of polyaniline films prepared in solutions of strong and weak acids and in water – FTIR and Raman spectroscopic studies, Polym. Degrad. Stabil. 93 (2008) 2147–2157.
[53] X. Feng, N. Chen, J. Zhou, Y. Li, Z. Huang, L. Zhang, Y. Ma, L. Wang, X. Yan, Facile synthesis of shape-controlled graphene–polyaniline composites for high performance supercapacitor electrode materials, New J. Chem. 39 (2015) 2261–2268.
[54] Y. Furukawa, F. Ueda, Y. Hyodo, I. Harada, T. Nakajima, T. Kawagoe, Vibrational spectra and structure of polyaniline, Macromolecules 21 (1988) 1297–1305.
[55] Z. Wu, S. Zhu, X. Dong, Y. Yao, Y. Guo, S. Gu, Z. Zhou, A facile method to graphene oxide/polyaniline nanocomposite with sandwich-like structure for enhanced electrical properties of humidity detection, Anal. Chim. Acta 1080 (2019) 178–188.
[56] H. Wang, Q. Hao, X. Yang, L. Lu, X. Wang, Graphene oxide doped polyaniline for supercapacitors, Electrochem. Commun. 11 (2009) 1158–1161.
[57] P. Pachfule, D. Shinde, M. Majumder, Q. Xu, Fabrication of carbon nanorods and graphene nanoribbons from a metal–organic framework, Nat. Chem. 8 (2016) 718–724.
[58] M. Hassan, K.R. Reddy, E. Haque, S.N. Faisal, S. Ghasemi, A.I. Minett, V.G. Gomes, Hierarchical assembly of graphene/polyaniline nanostructures to synthesize free-standing supercapacitor electrode, Compos. Sci. Technol. 98 (2014) 1–8.
[59] D. Shao, G. Hou, J. Li, T. Wen, X. Ren, X. Wang, PANI/GO as a super adsorbent for the selective adsorption of uranium(VI), Chem. Eng. J. 255 (2014) 604–612.
[60] K. Urbas, M. Aleksandrzak, M. Jedrzejczak, M. Jedrzejczak, R. Rakoczy, X. Chen, E. Mijowska, Chemical and magnetic functionalization of graphene oxide as a route to enhance its biocompatibility, Nanoscale Res. Lett. 9 (2014) 656.
[61] E.A. Sanches, J.M.S. da Silva, J.M. de O. Ferreira, J.C. Soares, A.L. dos Santos, G. Trovati, E.G.R. Fernandes, Y.P. Mascarenhas, Nanostructured Polyaniline Emeraldine-base form (EB-PANI): a structural investigation for different neutralization times, J. Mol. Struct. 1074 (2014) 732–737.
[62] X. Wang, L. Miao, C. Liu, J. Gao, Y. Chen, Thermoelectric enhancement of polyaniline grafting from graphene oxide, Mater. Sci. Forum 847 (2016) 153–160.
[63] J. Kang, J. Sheng, J. Xie, H. Ye, J. Chen, X.-Z. Fu, G. Du, R. Sun, C.-P. Wong, Tubular Cu(OH)2 arrays decorated with nanothorny Co–Ni bimetallic carbonate hydroxide supported on Cu foam: a 3D hierarchical core–shell efficient electrocatalyst for the oxygen evolution reaction, J. Mater. Chem. A 6 (2018) 10064–10073.
[64] M.U. Shahid, N.M. Mohamed, A.S. Muhsan, R. Bashiri, A.E. Shamsudin, S.N. A. Zaine, Few-layer graphene supported polyaniline (PANI) film as a transparent counter electrode for dye-sensitized solar cells, Diam. Relat. Mater. 94 (2019) 242–251.
[65] S. Park, R.S. Ruoff, Chemical methods for the production of graphenes, Nat. Nanotechnol. 4 (2009) 217–224.
[66] W.R. Bowen, T.A. Doneva, J.A.G. Stoton, Protein deposition during cross-flow membrane filtration: AFM studies and flux loss, Colloids Surf. B Biointerfaces 27 (2003) 103–113.
[67] D. Quéré, Wetting and roughness, Annu. Rev. Mater. Res. 38 (2008) 71–99.
[68] C.E. Goodyer, A.L. Bunge, Mass transfer through membranes with surface roughness, J. Membr. Sci. 409–410 (2012) 127–136.
[69] L. Xu, S. Shahid, A.K. Holda, E.A.C. Emanuelsson, D.A. Patterson, Stimuli responsive conductive polyaniline membrane: in-filtration electrical tuneability of flux and MWCO, J. Membr. Sci. 552 (2018) 153–166.
[70] J. Yin, G. Zhu, B. Deng, Graphene oxide (GO) enhanced polyamide (PA) thin-film nanocomposite (TFN) membrane for water purification, Desalination 379 (2016) 93–101.
[71] P. Bhol, S. Yadav, A. Altaee, M. Saxena, P.K. Misra, A.K. Samal, Graphene-based membranes for water and wastewater treatment: a review, ACS Appl. Nano Mater. 4 (2021) 3274–3293.
[72] Y. Zhou, M. Xia, Y. Ye, C. Hu, Antimicrobial ability of Cu2+-montmorillonite, Appl. Clay Sci. 27 (2004) 215–218.
[73] N.L. Shi, X.M. Guo, H.M. Jing, J. Gong, C. Sun, K. Yang, Antibacterial effect of the conducting polyaniline, J. Mater. Sci. Technol. 22 (2006) 289–290.